RSC Advances

ROYAL SOCIETY OF CHEMISTRY

www.rsc.org/advances

Rapid Osteogenic Differentiation of Mesenchymal Stem Cells on Hydroxyapatite Nanocrystal Clusters-Oriented Nanotopography

Ying Chen, Zhihui Sun, Yanyan Li, and Youliang Hong

The randomly-oriented HAP nanocrystal clusters-constructed nanotopography, prepared via a nucleation-oriented aggregation-recrystallization process from the HAP slices, can dictate BM-MSCs to differentiate into osteogenic lineages rapidly.

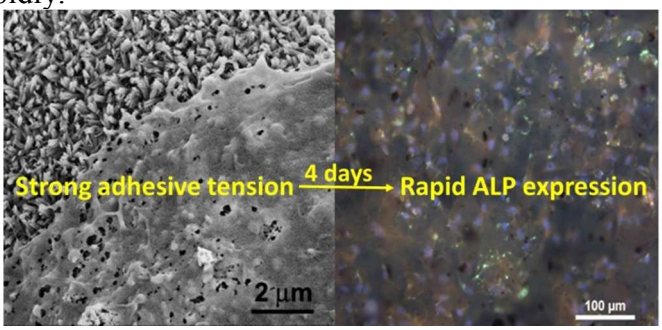

Journal Name

RSCPublishing

ARTICLE

Rapid Osteogenic Differentiation of Mesenchymal Stem Cells on Hydroxyapatite Nanocrystal Clusters-Oriented Nanotopography

Ying Chen[a], Zhihui Sun[b], Yanyan Li[b], and Youliang Hong[a*]

Cite this: DOI: 10.1039/x0xx00000x

Received 00th January 2012,
Accepted 00th January 2012

DOI: 10.1039/x0xx00000x

www.rsc.org/

Although it has been well demonstrated that specific nanotopographies alone can direct the fate decision of stem cells, it still has a huge gap, and at the same time, also denotes a large challenge to translate this concept into clinical trials. Herein, we reported on using a kind of clinically relative biomaterials, hydroxyapatite, to prepare a kind of specific nanotopography constructed by the randomly-oriented hydroxyapatite nanocrystal clusters, through high temperature water vapour treatment of the plasma-sprayed hydroxyapatite slices. Cell experiments demonstrated that bone-marrow mesenchymal stem cells could exert a strong adhesive tension on the nanocrystal clusters-oriented topography, and the formed strong intracytoskeletal stress in turn promoted cells to osteogenic differentiation rapidly and the differentiation process was associated with but faster than the model of osteoblastic differentiation. Therefore, our work reported here extremely shortened the gap of from the concepts of mechanotransduction, i.e., extracellular physical forces sponsored from materials features can induce the mechanochemical conversion to alter the fate decision of stem cells, to the clinical trials.

Introduction

Design and fabrication of biomaterials with specific signals to regulate the commitment of stem cells towards desirable lineage are becoming an exciting research area in tissue engineering and regenerative medicine. To this end, a variety of biological, chemical and physical strategies have been attempting, such as the incorporation of chemical/growth factors into biomaterial matrixes (e.g., BMP-2 is embedded into PLLA),[1,2] surface modification of biomaterials with functional groups (e.g., graft RGD on PLLA surface),[3,4] construction of special surface geometric feature,[5,6] topography and roughness,[7-11] modulation of substrate elasticity,[12,13] etc. Among these approaches, physical cues arisen from micro-/nanoscale topography and roughness are particularly attractive because unlike chemical/growth factors, the micro-/nanotopographies control nothing more than stem cell fate, not having the in vivo variability and potential side effects associated with chemical additions, and thereby being more dependable than chemical/growth factors.[14]

In the use of topographical cues to direct the fate decision of stem cells, recent studies have demonstrated that several kinds of micro-/nanotopographies, e.g., disordered pits,[7] pillars,[8] surface oriented nanotubes[14] or nanowires,[15] etc., could induce mesenchymal stem cells (MSCs), a kind of multipotent stem cells, to produce targeted osteogenic lineages. These findings would be very useful guidance, at the same time, also presented good perspective for a range of applications in regenerative medicine of orthopedics and dentistry. Especially, because there are abundant MSCs in bone marrow, the MSCs can easily arrive at and interact with the topography of biomaterials implanted at the site of bone defect. Thus, the cost (including cell harvest and in vitro culture) and risk (e.g., immunologic rejection, mutation, etc.) of using the isolated cells can be eliminated completely. Nevertheless, there are huge obstacles that the currently-reported topographies can be applied for clinical practice, mainly because scaling up production of nanotopographies based on current techniques, e.g., photolithography,[16] electron beam lithography,[17] soft lithography,[18] etc., for the generation of whole devices presents logistical challenges; In addition, most of currently-reported substrates for patterning nanotopographies are not clinically relevant materials.[7,14,15] Therefore, it is still great challenge to supply this gap through seeking available processing techniques to tailor orthopedic and dental relevant materials.

Hydroxyapatite (HAP), due to similar chemistry with mineral phase of bone, excellent biocompatibility, good bioactivity and osteoconductivity, has been widely used as clinical materials for orthopedic and dental surgery.[19,20] Still, current HAP bioceramics have low biological performances, and hardly have ability to guide the regeneration of defective hard tissues, which extremely weaken their clinical applications, especially, limiting their usage in reconstruction of large bone defects. Therefore, continuous efforts to extend the biological potentials of the HAP ceramics become of center importance. Herein, we report a kind of HAP nanotopography constructed by the oriented HAP nanocrystal clusters. The cell experiments

demonstrated that this nanotopography could regulate osteogenic differentiation of MSCs rapidly.

Experimental

Materials

The well-crystallized HAP powders with average diameter <40 μm were synthesized in our lab according to the precipitation method and sintered at 1100 °C. The commercial Ti plates were used. The deionized water was used in the whole experiments. In light of experiment demands, the Ti plates were processed into discs (ø 14×1 mm).

Preparation of the HAP nanocrystal clusters-oriented slices

In a typical process, the HAP powders were sprayed to smooth Ti substrates under nitrogen gas protection with the following spray parameters: applied power: 24 kW, spray distance: 16 cm, plasma gas: argon (50 L/min)/hydrogen (5 L/min), and transport gas for spheres: 1.5 L/min. Once the spray process finished, the heat samples (500-600 °C. these samples have been heated during spraying) were exposed to air at once. The as-sprayed HAP slices were further treated under 130 °C water vapour circumstances (The schematic illustration of the device for water vapour treatment is shown in Fig. S1, supporting information) for 2 h to achieve the HAP nanocrystal clusters-oriented slices. In a control experiment, i.e., the 120 °C and 150 °C water vapour treatments were carried out to observe whether the morphology of the HAP nanocrystal clusters will change. The vapour treated samples were then characterized using a scanning electron microscope (SEM, Hitachi S-4800), Transmission electron microscope (TEM, Tecnai G2 F20 S-TWIN, FEI), X-ray diffraction (XRD, X'Pert Pro MPD, Philips). The elastic moduli of samples were evaluated by three-point bending test.

Cell culture

Bone marrow MSCs were harvested from thigh-bones of neonatal rabbits. The harvested MSCs were passaged and the passage 3 MSCs were used to seed onto samples. The culture medium was a mixed system of α-MEM (89 vol.%), fetal bovine serum (10 vol.%, FBS; Gibco, USA), and penicillin–streptomycin (1 vol.%, PS; Gibco, USA). After sterilization, the samples were placed in the 24-well plates (Corning, USA) and seeded with 2×10^4 cells/well in 2 mL of medium. Then the cell-seeded samples were cultured at 37 °C in a humid, 5 % CO_2-contained atmosphere. The culture media were changed at intervals of 3 days and the samples were removed at defined time point for biological analyses.

Live-dead analyses

The MSCs cultured in different scaffolds over time were observed by a confocal laser scanning microscopy (CLSM, Olympus IX 95). Before observation, the cell-adhered scaffolds were rinsed by sterile phosphate buffered saline (PBS) and stained by fluoresein diacetate (FDA) for live cells and propidium iodide (PI) for dead cells.

SEM of cells

Adherent cells on samples were fixed with 2.5% glutaraldehyde for 4 h. After washing with Mili-Q water, the cells were dehydrated in a graded ethanol series from water through 10%, 20%, 50%, 75%, 80%, and 95% ethanol with time interval 15 min, and last through 100% ethanol for 30 min. The samples then were placed in a critical point drying apparatus (Hitachi), where ethanol was replaced with liquid CO_2, which was heated to 27 °C and changed state to its gaseous phase. The CO_2 gas was vented and then samples coated with gold using sputter coater. The samples were tested using SEM.

Phalloidin staining

The cultured cells were rinsed two times using PBS briefly to remove media components, and then cells were fixed in 3.7% formaldehyde in PBS (freshly prepared) for 5 min at room temperature and washed 3 times in PBS. Cells were dehydrated with acetone, permeabilized with 0.1% Triton X-100 in PBS, and washed again in PBS. Cells were stained with a 50 mg/ml rhodamine-phalloidin conjugate (Sigma, Catalog Number P1951) solution in PBS (containing 1% DMSO from the original stock solution) for 40 minutes at room temperature. The samples were washed 3 times with PBS to remove unbound phalloidin conjugate and the nuclei were stained with DAPI at 37 °C.

Alkaline phosphatase staining

Cells were stained for alkaline phosphatase (ALP) using Sigma kit number 86C according to the manufacturer's instructions.

Von Kossa staining

After 14 days, the cultured cells have washed 3 times using ice-cold PBS, fixed with 3.7% formaldehyde for 1 h. Samples were stained in 5% silver nitrate for 1 h, then exposed to ultraviolet light, and last counterstained with 1% neutral red.

Osteogenesis-related gene expression

The expressions of osteogenesis-related genes were evaluated by quantitative real-time polymerase chain reaction (QRT-PCR). The cells cultured on samples for 4, 7, and 14 days were rinsed twice with PBS and their total RNA was isolated using the Trizol reagent (Invitrogen, Carlsbad, CA) according to the manufacturer's protocol and collected by ethanol precipitation. 1 μg RNA from each sample was reversed transcribed into complementary DNA (cDNA) using an iScript cDNA Synthesis Kit (Bio-Rad, CA). Equal volumes of cDNA were used to program QRT-PCR reactions specific for some osteogenesis-related mRNAs encoding, including core-binding factor alpha-1 (Cbfa-1), bone morphogenetic protein-2 (BMP-2), osteopontin (OPN), collagen-I (COL-I),bone sialoprotein (BSP), and osteocalcin (OCN). Forward and reverse primers for the selected genes were designed and are listed in Table S1.

Reactions were performed using PCR Tube Strips (TCS0803) (Bio-Rad, CA) and thermocycling in a CFX96 real time thermocycler (Bio-Rad, CA). Relative mRNA abundance was determined by the 2-ΔΔCt method and reported as fold induction. GAPDH abundance was used for normalization. The obtained results then were normalized by the live cell numbers.

Statistical analysis

All data were presented as means ± standard deviations (S.D.). To test the signification of observed differences between the study groups, an unpaired Student t-test was applied. A value of $p < 0.05$ was considered to be statistically significant.

Results

Preparation of the HAP nanocrystal clusters-oriented nanotopography

To achieve the HAP nanocrystal clusters-oriented topography, in our experiment the HAP slices prepared by atmospherically plasma spraying the HAP powders were used as primary materials. SEM images (Fig. 1a-b) show that the surface of the as-sprayed HAP slices is smooth at micro-/nanoscale, but roughness at macro-/microscale. The XRD pattern shown in Fig. 2(a-i) reveals that the HAP slice was composed of the crystalline HAP, amorphous calcium phosphate and some other crystalline phases including α-tricalcium phosphate (α-TCP), tetracalcium phosphate (TTCP) and calcium oxide (CaO). The formation of amorphous calcium phosphate and non-HAP phases is attributable to rapid melting-solidification and thermal decomposition of HAP during plasma spraying.[21]

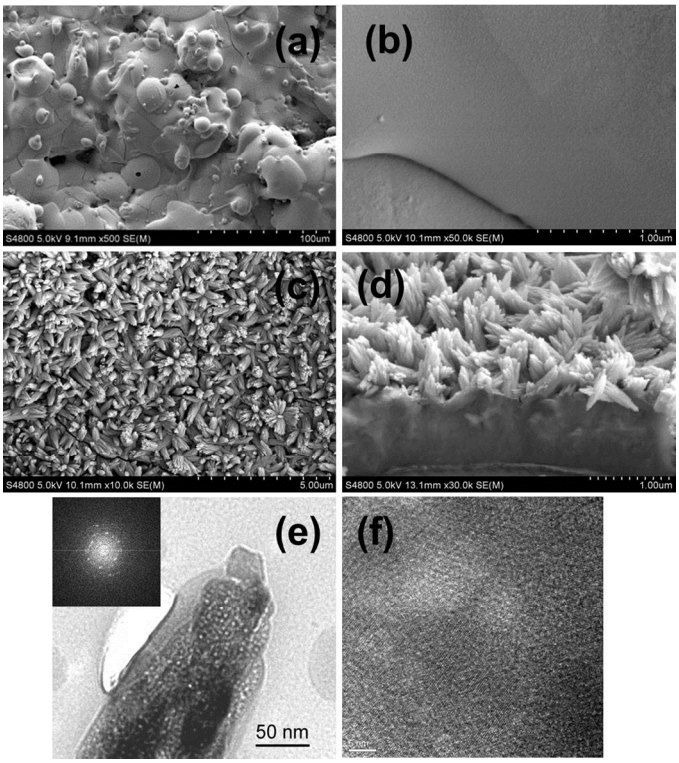

Fig. 1. (a, b) SEM images of the plasma-sprayed HAP slice, (c, d) the HAP nanocrystal clusters formed and oriented randomly towards the HAP slice surface, (e) TEM image and SEAD pattern (inserted) of the HAP nanocrystal clusters, (f) high resolution TEM image of the HAP nanocrystal clusters.

After the HAP slices were further treated under the 130 °C water vapour condition for 2 h, the nanorods formed and oriented randomly toward the slice surface, as shown in Fig. 1(c-d). The magnified image (Fig. 3c) shows that the formed nanorods in fact are a kind of nanocrystal clusters with average diameter ~250 nm, average length ~ 800 nm, consisting of some smaller nanocrystals. TEM image (Fig. 1e) and high resolution TEM (Fig. 1f) and the selected area electron diffraction (SEAD) pattern inserted in Fig. 1(d) further demonstrate that the nanocrystal clusters consist of packed small nanocrystals. The XRD pattern (Fig. 2a-ii) verified that all non-HAP phases and amorphous calcium phosphate in the slices have been converted into well-crystallized HAP phase, which also suggests that the formed nanocrystal clusters are composed of HAP. FTIR result (Fig. 2b) shows that the intensity of –OH group peak at 3574 and 630 cm^{-1} increased after water vapour-treatment, further demonstrating that the increase of HAP amount in system. The conversion of non-HAP phases can be well understood because the non-HAP phases, including α-TCP, TTCP, and CaO, have far higher solubility than HAP under aqueous media, and surely react with water under high temperature condition to form the stablest HAP phase.[19]

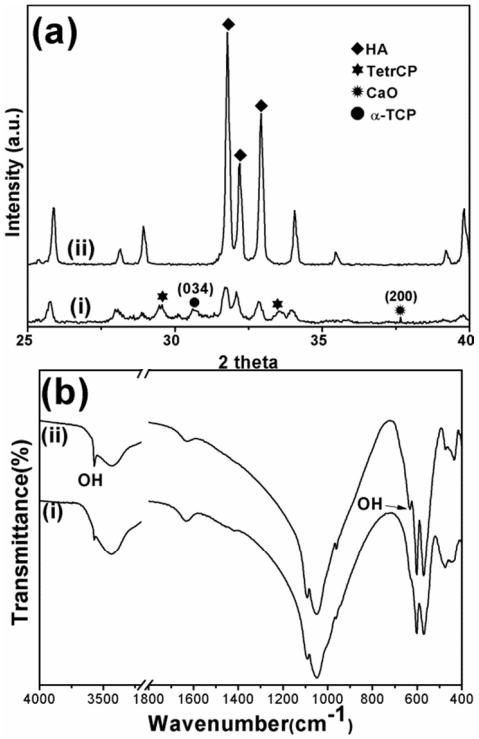

Fig. 2. (a) XRD pattern and (b) FTIR of (i) as-sprayed and (ii) 130 °C water vapour-treated HAP slices.

To understand the formation mechanism of the randomly-oriented HAP nanocrystal clusters, their growth process was investigated over time. Fig. 3 shows that their growth goes through a typical self-assembling process and abides by a nucleation-oriented aggregation-recrystallization mechanism under high temperature water vapour circumstance.[22-24] In brief, primary HAP nanocrystals firstly nucleate and reside on the slice surface in a supersaturated state resulted from the water vapour-induced release of the non-HAP phases from slice (Fig. 3a). As the reaction goes on, more non-HAP components dissolve and nucleate into the HAP nanocrystals. Due to high surface energy, the newly formed nanocrystals have high potential to spontaneously aggregate and oriented-attachment by an orderly way so that the nanocrystals share a common crystallographic orientation (Fig. 3b).[25-27] The spontaneously-assembled aggregates, under high temperature circumstance would continuously recrystallize to improve their crystallinity and form the HAP nanocrystal clusters (Fig. 3c).

Experiments indicated that the morphology of the HAP nanocrystal clusters was depended on the temperature. As can be seen from Fig. 3(d), when the HAP slices were treated under a higher water vapour condition, i.e., 150 °C, for 2 h, the

formed nanocrystal-clusters presented a relatively dispersive cluster structure, and in a nanocrystal cluster the small nanocrystals showed longer length. In contrast, the crystallinity of the nanocrystal clusters could enhance when a low water vapour temperature was employed. As shown in Fig. 3(e), when the HAP slices were treated under 120 °C water vapour condition for 4 h, the grown clusters almost formed the typical hexagonal HAP monocrystals, and the single small crystals in a cluster hardly be observed. Above results suggested that the high temperature will improve the crystallinity of primary HAP nanocrystals and decrease their surface energy, thus decreasing the aggregation of primary nanocrystals. On the contrary, under the low temperature, the primary nanocrystals will have low crystallinity and high surface energy, thereby the primary nanocrystals easily aggregate and recrystallize.

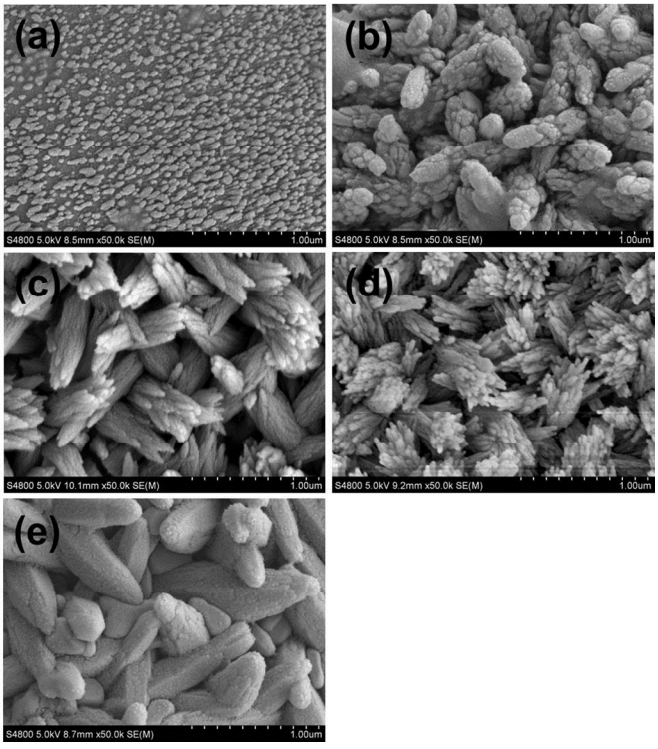

Fig. 3. SEM images of the as-sprayed HAP slices suffered from (a) 10 min, (b) 1.0 h, and (c) 2.0 h of 130 °C water vapour treatment, and (d) 150 °C water vapour treatment for 2 h, and (e) 120 °C water vapour treatment for 4 h.

Survival and proliferation of MSCs

The as-prepared HAP nanocrystal clusters (130 °C for 2h) then were used to culture with bone marrow MSCs of rabbits. At first we investigate the survival and proliferation of MSCs on our samples. The experiments showed that the nanotopographies affected the survival and proliferation of MSCs. As can be seen from Fig. 4, at early stage, the proliferation rate of cells on the nanotopographies was lower than that on the smooth HAP surface. Still, with another 3 day culture, the number of cells on the nanotopographies increased largely and reached the same level with that cultured on the smooth surface. At the same time, Fig. 4 shows that higher dead rate was presented on the nanotopographies than on the smooth HAP surface within 10 days.

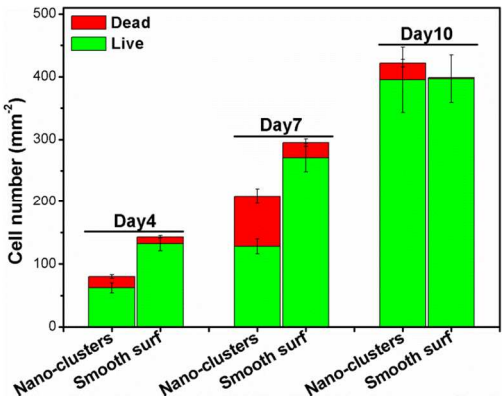

Fig. 4. Live-dead staining of cells adhered on the HAP nanocrystal-clusters and the smooth HAP surfaces over time (mean±S.D., n=4).

Surface spreading of MSCs

SEM image (Fig. 5a1) shows that MSCs could fully spread on the mixed micro- and nanotopographies and presented a strong adhesive tension. The magnified SEM image (Fig. 5a2) shows that in microscale area, some small filopodia adhered around the nanocrystal clusters and imprints of clusters in the lamellae could be observed (black arrows). The presentation of cluster imprints in cell membranes suggested that cells attempt to endocytose these nanocrystal clusters.[28] Phalloidin staining (Fig. 5a3) indicates that MSCs could assemble a cortical F-actin cytoskeleton through the cytoplasm and the organized cytoskeleton filaments were tense. Furthermore, the immunofluorescence staining of non-muscle myosin IIa (Fig. 5a4), a kind of actin-binding motor protein that binds and cross-links actin filaments and then mediates sliding of anti-parallel actin filaments during contraction of stress fibers and thereby increasing endogenous cell tension,[29-31] clearly indicates that high-levels of myosin IIa were expressed by the cells adhered on the HAP nanocrystal-clusters.

By comparison, a control experiment was carried out by culturing MSCs on the surface of the HAP slices that had not suffered from high temperature water-vapour treatment. Fig. 5(b1) shows that MSCs also could spread well on such smooth surface and abundant and long filopodia (Fig. 5b2) were presented on the smooth surface. Still, phalloidin staining (Fig. 5b3) shows that few stress fibers were concentrated and the concentrated stress fibers were relaxant (Fig. 5b3), and non-muscle myosin IIa staining shows that low-levels of myosin IIa expression (Fig. 5b4).

Osteogenic differentiation of MSCs

Subsequently, ALP activity of MSCs cultured on the HAP substrates was monitored over time. ALP is used because ALP is a potent and significant predictor of osteogenic lineage commitment, and also is a highly specific marker and inducer of bone formation.[32] Very interestingly and fortunately, at day 4, the ALP expressed by MSCs, but still stayed inside MSCs was captured, as shown in Fig. 6(a1) (Fig. S2 shows the magnified image, see supporting information). Fig. 6(c1) shows that the expressed ALP is very high (78%). It verified that the MSCs regulated by the HAP nanocrystal clusters started to express ALP at day 4 accurately. To best of our knowledge, it is the fastest that the nanotopography alone induces MSCs to differentiate into osteogenic lineages and express ALP. After 7 day culture, higher amount of ALP (94%) secreted out of cells were observed (Fig. 6a2&c2). By comparison, cells cultured on

the smooth HAP slices hardly expressed ALP at day 4 (Fig. 6b1&c1) and a little at day 7 (Fig. 6b2&c2).

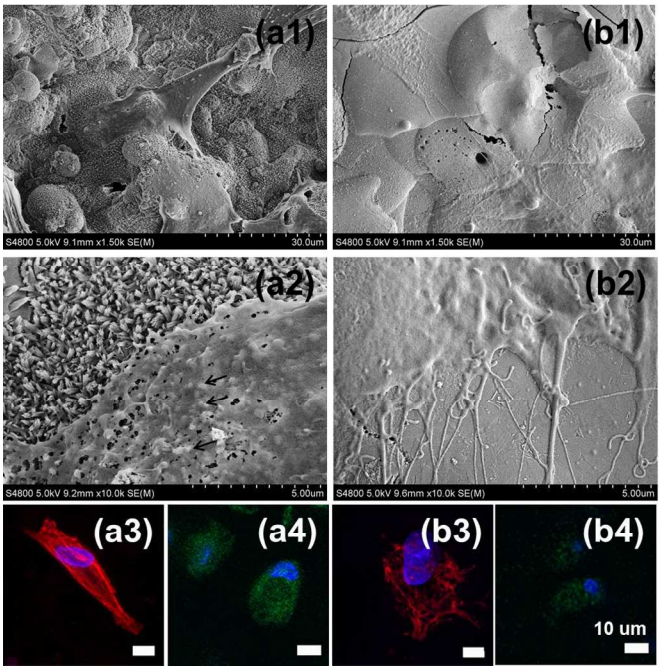

Fig. 5. Spreading and cytoskeletal organization of MSCs. SEM images (a1-b2), phalloidin staining (a3, b3), and immunofluorescence staining (a4, b4) of MSC responding to the HAP nanocrystal clusters oriented surface (a1-a4) and the as-sprayed HAP surface (b1-b4).

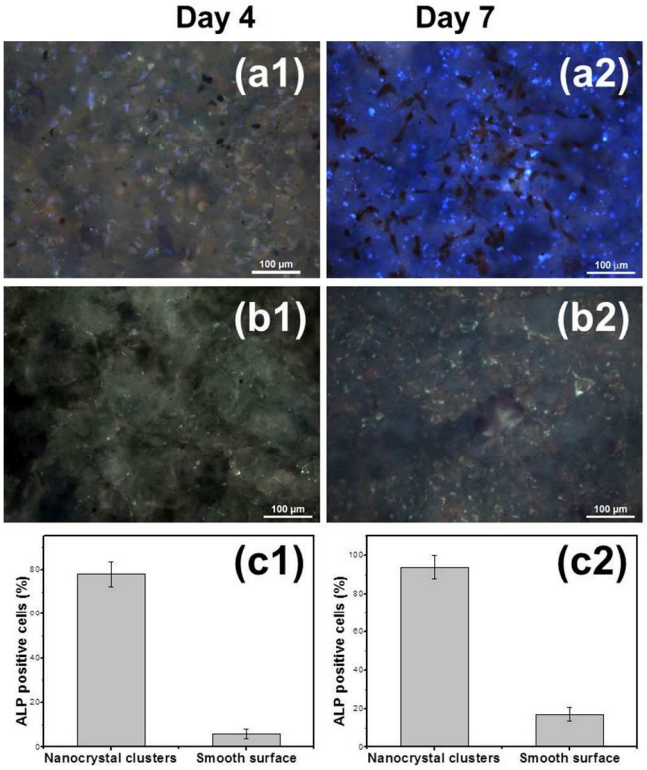

Fig. 6. ALP staining of MSCs cultured on the HAP nanocrystal clusters (a1, a2) and on the smooth HAP surface (b1, b2) at day 4 (a1, b1) and day 7 (a2, b2). Quantification of ALP expression at day 4 (c1) and day 7 (c2); mean ± S.D.

At day 14, cells cultured on the HAP nanocrystal clusters expressed abundant mineral nodules (Fig. 7 a1&a2), but not on the smooth HAP slices (Fig. 7b1&b2). The formation of mineral nodules further verified the osteogenic differentiation of MSCs mediated by the HAP nanocrystal clusters.

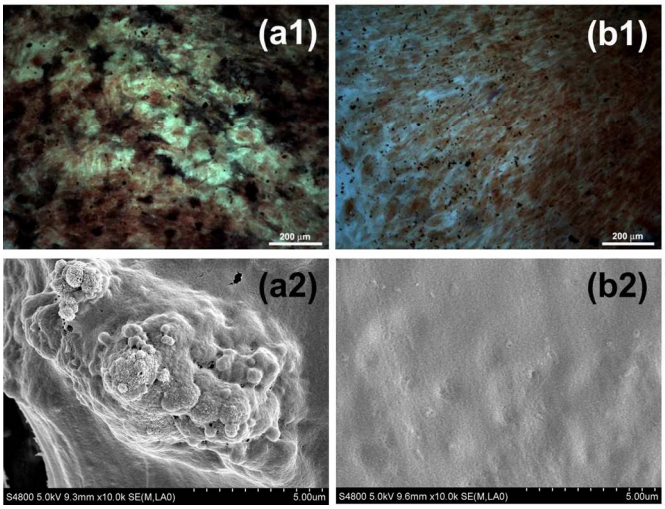

Fig. 7. The formation of mineral nodules. Von Kossa staining (a1, b1) and SEM images (a2, b2) showed that mineral nodules were formed at day 14 on the nanocrystal clusters (a1, a2) but not on the smooth HAP surface (b1, b2).

Fig. 8 shows the gene expressions of MSCs on two kinds of samples over time. The cells expressed highest level of Cbfa-1 (Fig. 8a), which is early maker mRNAs of osteoblast differentiation, at early stage on the nanocrystal clusters when comparing the smooth HAP surface, and then the level of these gene expressions down-regulated continuously over 14 days. BMP-2 (Fig. 8b), another specific osteogenic marker, also was expressed by cells on the HAP nanotopographies at early stage, and the expression level begun to down-regulated from day 7. In contrast, the expression levels of Cbfa-1 and BMP-2 were always very low within 14 days by cells adhered on the smooth HAP surface. Similar from Cbfa-1 and BMP-2, the expression of Col-I by the cells cultured on both samples increased at first and then decreased (Fig. 8c). Furthermore, the expressed level of Col-I on the nanotopographies is higher than that on the smooth HAP surface. Still, the expression quantity of Col-I is higher than Cbfa1 and BMp-2. Such result suggested that the matrix has small influence on the expression of Col-I. OPN, responsible for calcium ion binding, is generally used as a terminal maker of osteoblast differentiation.[33] The expression of OPN on the HAP nanotopographies increased at day 7 and then decreased (Fig. 8d). The high expression of OPN in the nanocrystal clusters can be concluded as the formation of the bone-like mineral nodules on the sample surfaces, as demonstrated in Fig. 7(a1&a2). In contrast, no OPN was expressed by cells on the smooth HAP surface in the whole culture period, which well corresponded with the results shown in Fig. 7(b1&b2). Another two kinds of mineral-relative genes, BSP and OCN,[34,35] both were expressed highly on the nanocrystal-clusters at day 7 but were not on the smooth surface. Such results further demonstrated the formation of

mineral nodules as shown in Figure 7. Especially, because OCN only can be expressed by osteoblasts,[35] the MSCs adhered on the surface of nanocrystal-clusters surely have differentiated into osteoblasts.

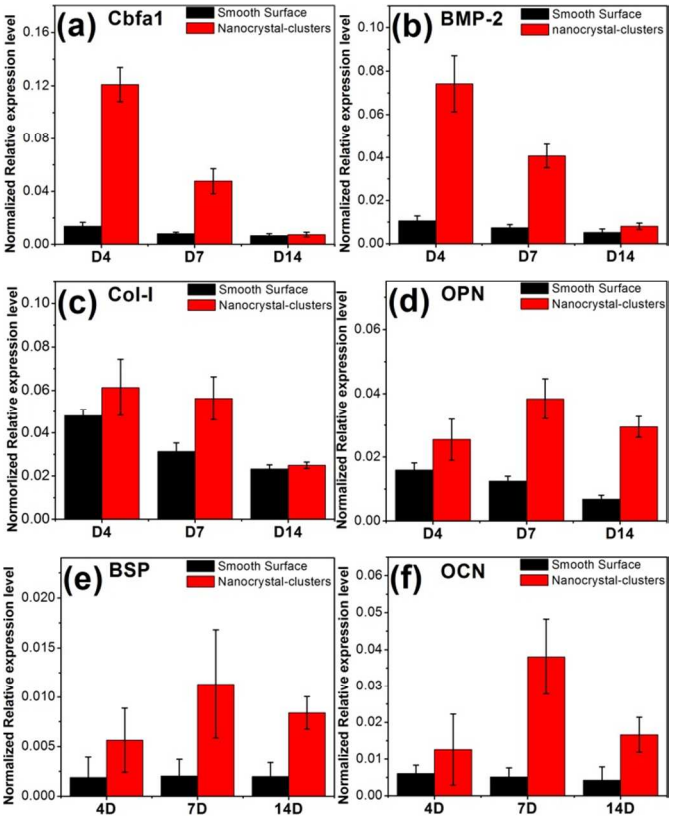

Fig. 8 QRT-PCR results of cells cultured on the HAP nanocrystal-clusters and smooth HAP surface over time (mean±S.D., n=3).

Discussion

It is well known that cells are sensitive to substrate stiffness/rigidity, and when the substrate stiffness is high enough (e.g., the elastic moduli > 30 kPa), cells trend to spread on its surface.[12] In our samples, because the mechanical stiffness of both samples believed is far higher than 30 kPa,[37] they facilitated MSCs to spread and organize actin fibres. However, in addition to the substrate stiffness, the mixed HAP topographies bear microscale roughness, nanoscale nanocrystal clusters, and abundant Ca-/P-sites from HAP,[20] which also largely contribute the formation of strong cell tension. Among these factors, the roles of nanocrystal clusters seem to be dominative because the control experiments have indicated that microscale roughness and Ca-/P-sites could not produce strong adhesive tension. Although the HAP has abundant Ca- and P-sites to interact with those cellular proteins distributed at extracellular domains, the cell-nanoscale smooth surface connection demonstrated was a little weaker than the specific RGD molecular bonds (e.g., RGD-integrin interaction).[38] The full spreading of cells on the control HAP samples implicated that the smooth HAP slice is a compliant substrate, on which MSCs just assemble the cytoskeleton to keep an adhesion/tension balance.[39] The expression of many filopodia on the smooth HAP surface seems to confirm our hypothesis. In general, cells would assemble filopodia to probe their microenvironment.[40] The smooth HAP surface could promote cells to assemble filopodia to "search" the anchor sites, but due to the lack of the anchor sites, the assembled filopodia could not promote the organized cytoskeletal filaments to produce a high-enough tensed cytoskeletal force. In the nanotopography constructed by the HAP nanocrystal clusters, besides the Ca-/P-site-protein interactions, however, the nanocrystal clusters provided sites for cell adhesion and stretch to expand the initial adhesion spot and mimic an endocytic process, which then would be associated with local mechanical stresses and cytoskeletal organization.[41]

Taken together, above analyses confirm that the MSCs adhered on the HAP nanocrystal-clusters can differentiate into osteogenic lineage rapidly, and the differentiation process is associated with but faster than the model of osteoblastic differentiation.[36]

The rapid osteogenic differentiation of MSCs shown here well demonstrated that cellular mechanotransduction based on extracellular physical forces originated from the HAP nanocrystal clusters to transfer cues is faster than the chemical/growth factors.[42] Because the oriented nanocrystal clusters exerted a strong traction force to tense the cytoskeletal filaments of cells, the mechanical stress could be propagated along tensed cytoskeletal filaments in a long distance to nucleus to alter molecular self-assembly events and modulate nuclear biochemistry by many possible mechanisms,[43-45] thus triggering downstream signalling cascades that lead to force-dependent changes in gene expression. By contrast, in the cells spread on the smooth HAP slice, the cytoskeleton network is relaxant. The mechanical stress exerted to the relaxant cytoskeletal filaments decayed rapidly over a short distance in space; thereby the stress could not be propagated to nuclear.

It should be pointed out that previously Engler et al have reported that the substrates with high stiffness (25-40 KPa) (in fact the substrate was composed of collagen I coated polyacrylamide) could induce MSCs to commit towards osteogenic lineages.[13] However, later Rowlands et al have further supplemented this experiment using same substrates in which they demonstrated that it was not the substrate stiffness alone, but the combinations of substrate stiffness and collagen I (Collagen I contains abundant ligands for specific interaction with cellular surface membrane receptors, such as integrins and cadherins) that could mediate MSCs to differentiate.[46] Indeed, because lacking the matrix ligands, our smooth HAP slices verified also could not mediate MSC adhesion to produce the tensed intracytoskeletal stress and subsequently differentiate in spite of high stiffness. Nevertheless, in the HAP nanotopographies, the nanotopographies alone could mediate cell adhesion and differentiation. It is speculated that small filopodia adhering around and attempting to endocytose the nanocrystal clusters could favour the recruitment of adhesive molecules to increase cell adhesion and therefore could exert significant traction forces.[41]

In comparison with other osteoinductive nanotopographies, e.g., the disordered nanopits,[7] in which the osteogenic commitment of MSCs occurred at day 7, our nanotopographies could induce the osteogenic commitment of MSCs is more rapidly. A possible explanation is that our nanotopographies could mediate the spread MSCs to form a stronger cytoskeleton tension resulted from filopodia adhering around and attempting to endocytose the nanocrystal clusters. The stronger tension, of course, could transmit the mechanical stress more rapidly to nucleus. Still, more experiments need be carried out to clarify this biological mechanism.

It is well known that HAP possesses excellent bio-compatibility because of its similarity as the minerals of bone. However, our results showed that when HAP is tailored into the nanocrystal-clusters, the survival rate and proliferation of cells decreased at early stage. The slow cell proliferation could be attributed to the osteogenic differentiation of MSCs. Generally, during cellular differentiation, its proliferation rate will decrease.[47] The relatively high dead rate speculated resulted from some cuspidal tops of the nanocrystal-clusters, which easily puncture cells and influenced cell locomotion. Nevertheless, such drop is not essential to influence cell proliferation and osteogenic differentiation. As shown in Fig. 8, the cell number increased to the same level with the smooth surface at day 10.

Conclusions

In summary, we have successfully tailored the clinical-related biomaterials, HAP, into the randomly oriented nanocrystal cluster-constructed nanotopographies, by high temperature water vapour treating the plasma sprayed HAP slices. In vitro experiments have verified that such nano-topographies alone could rapidly induce MSCs to express ALP at day 4, mineral nodules at day 14, and osteoblast-relative genes during differentiation, thereby demonstrating rapid osteogenic differentiation of MSCs, and thereby our HAP nano-topographies are osteoinductive. Because HAP has been widely applied as filling materials in orthopaedic surgery, especially, the HAP coated Ti has been well used as hip replacements, we believe that our HAP nanotopographies could easily are associated with clinical trials in the orthopaedic surgery.

Acknowledgements

This work was supported by National Natural Science Foundation of China (Grant 31170928).

Notes and references

[a] National Engineering Research Center for Biomaterials, Sichuan University, Chengdu, 610064, P. R. China

[b] Department of Pharmacy of the First Hospital, Jilin University, Changchun 130012, P. R. China.

Electronic Supplementary Information (ESI) available: The schematic illustration of the device for high temperature water-vapor treatment; The magnified ALP staining of MSCs cultured on the HAP nanocrystal clusters; and the Live-dead staining of MSCs cultured on both samples over time. See DOI: 10.1039/b000000x/

1 D. Schofer, P. P. Roessler, J. Schaefer, C. Theisen, S. Schlimme, J. T. Heverhagen, M. Voelker, R. Dersch, S. Agarwal, S. Fuchs-Winkelmann and J. R. J. Paletta, *PLoS One*, 2011, **6**, e25462.

2 J. Li , J. Hong, Q. Zheng, X. Guo, S. Lan, F. Cui, H. Pan, Z. Zou and C. Chen, *J. Orthop. Res.*, 2011, **29**, 1745.

3 J. R. Paletta, S. Bockelmann, A. Walz, C. Theisen, J. H. Wendorff, A. Greiner, S. Fuchs-Winkelmann and M. D. Schofer, *J. Mater. Sci. Mater. Med.*, 2010, **21**, 1363.

4 J. F. Alvarez-Barreto, B. Landy, S. VanGordon , L. Place , P. L, DeAngelis and V. I. Sikavitsas, *J. Tissue Eng. Regen. Med.*, 2011, **5**, 464.

5 R. McBeath, D. M. Pirone, C. M. Nelson, K. Bhadriraju and C. S. Chen, *Dev. Cell*, 2004, **6**, 483.

6 K. A. Kilian, B. Bugarija, B. T. Lahn and M. Mrksich, *Proc. Natl. Acad. Sci. USA*, 2010, **107**, 4872.

7 M. J. Dalby, N. Gadegaard, R. Tare, A. Andar, M. O. Riehle, P. Herzyk, C. D. W. Wilkinson and R. O. C. Oreffo, *Nature Mater.*, 2007, **6**, 997.

8 T. Sjöström, M. J. Dalby, A. Hart, R. Tare, R. O.C. Oreffo and B. Su, *Acta Biomaterialia*, 2009, **5**, 1433.

9 F. Gentile, L. Tirinato, E. Battista, F. Causa, C. Liberale, E. M. di Fabrizio and P. Decuzzi, *Biomaterials*, 2010, **31**, 7205.

10 L. E.McNamara, R. J. McMurray, M. J. P. Biggs, F. Kantawong, R. O. C. Oreffo and M. J. Dalby, *J. Tissue Eng.*, 2010, **2010**, 120623.

11 C. J. Bettinger, R. Langer and J. T. Borenstein, *Angew. Chem. Int. Ed.*, 2009, **48**, 5406.

12 D. E. Discher, P. Janmey and Y. Wang, *Science*, 2005, **310**, 11393.

13 A. J. Engler, S. Sen, H. L. Sweeney and D. E. Discher, *Cell*, 2006, **126**, 677.

14 S. Oh, K. S. Brammer, Y. S. J. Li, D. Teng, A. J. Engler, S. Chien and S. Jin, *Proc. Natl. Acad. Sci. USA*, 2009, **106**, 2130.

15 S. W. Kuo, H. I. Lin, J. H. C. Ho, Y. R. V. Shih, H. F. Chen, T. J. Yen and O. K. Lee, *Biomaterials*, 2012, **33**, 5013.

16 P. Molna, W. S. Wang, A. Natarajan, J. W. Rumsey and J. J. Hickman, *Biotechnol. Prog.*, 2007, **23**, 265.

17 H. Hatakeyama, A. Kikuchi, M. Yamato and T. Okano, *Biomaterials*, 2007, **28**, 3632.

18 G. M. Whitesides, E. Ostuni, S. Takayama, X. Y. Jiang and D. E. Ingber, *Annu. Rev. Biomed. Eng.*, 2001, **3**, 335.

19 L. L. Hench, *J. Am. Ceram. Soc.*, 1998, **81**, 1705.

20 Y. Hong, H. Fan, B.Li, B. Guo, M. Liu and X. Zhang, *Mater. Sci. Eng. R*, 2010, **70**, 225.

21 R. B. Heimann and T. A. Vu, *J. Thermal Spray Technol.*, 1997, **6**,145.

22 X. L. Hu and J. C. Yu, *Adv. Funct. Mater.*, 2008, **18**, 880.

23 R. Q. Song and H. Cölfen, *Adv. Mater.*, 2010, **22**, 1301.

24 P. Simon, E. Rosseeva, I. A. Baburin, L. Liebscher, S. G. Hickey, R. Cardoso-Gil, A. Eychmüller, R. Kniep and W. Carrillo-Cabrera, *Angew. Chem. Int. Ed.*, 2012, **51**, 10776.

25 R. L. Penn and J. F. Banfield, *Science*, 1998, **281**, 969.

26 Y. Yin and A. P. Alivisatos, *Nature*, 2005, **437**, 664.

27 M. Niedergerge and H. Cölfen, *Phys. Chem. Chem. Phys.*, 2006, **8**, 3271.

28 M. J. Dalby, C. C. Berry, M. O. Riehle, D. S. Sutherland, H. Agheli and A. S. G. Curtis, *Exp. Cell Res.*, 2004, **295**, 387.

29 J. T. Parsons, A. R. Horwitz and M. A. Schwartz, *Nat. Rev. Mol. Cell Bio.*, 2010, **11**, 633.

30 R. Meili, B. A. Latorre, J. C. del Álamo, R. A. Firtel and J. C. Lasheras, *Mol. Bio. Cell*, 2010, **21**, 405.

31 M. V. Manzanares, X. Ma, R. S. Adelstein and A. R. Horwitz, Nat. Rev. Mol. Cell Bio., 2009, **10**, 778.

32 N. D. Escudero and P. M. Mandalunis, *Bone*, 2007, **40**, S7.

33 C. M. Giachelli, *Orthod. Craniofac. Res.*, 2005, **8**, 229.

34 G. K. Hunter and H. A. Goldberg, *Proc. Natl. Acad. Sci. USA*, 1993, **90**, 8562.

35 P. Ducy, C. Desbois, B. Boyce, G. Pinero, B. Story, C. Dunstan C, E. Smith, J. Bonadio, S. Goldstein, C. Gundberg, A. Bradley and G. Karsenty, *Nature*, 1996, **382**, 448.
36 G. S. Stein and J. B. Lian, *Endocr. Rev.*, 1993, **14**, 424.
37 C. Zhang, Y. Leng and X. Zhang, *J. Biomed. Mater. Res.*, 2000, **50**, 267.
38 A. A. Sawyer, K. M. Hennessy and S. L. Bellis, *Biomaterials*, 2005, **26**, 1467.
39 R. J. McMurray, N. Gadegaard, P. M. Tsimbouri, K. V. Burgess, L. E. McNamara, R. Tare, K. Murawski, E. Kingham, R. O. C. Oreffo and M. J. Dalby, *Nature Mater.*, 2011, **10**, 637.
40 P. K. Mattila and P Lappalainen, *Nat. Rev. Mol. Cell Biol.*, 2008, **9**, 446.
41 F. Gentile, L. Tirinato, E. Battista, F. Causa, C. Liberale, E. M. di Fabrizio and P. Decuzzi, *Biomaterials*, 2010, **31**, 7205.
42 N. Wang, J. D. Tytell and D.E. Ingber, *Nature Rev. Mol. Cell Biol.*, 2009, **10**, 75.
43 D. Stamenovic and D. E. Ingber, *Soft Matter*, 2009, **5**, 1137.
44 N. Itano, S. Okamoto, D. Zhang, S. A. Lipton and E. Ruoslahti, *Proc. Natl Acad. Sci. USA*, 2003, **100**, 5181.
45 A. G. Prat and H. F. Cantiello, *Am. J. Physiol*., 1996, **270**, C15323.
46 A. S. Rowlands, P. A. George and J. J. Cooper-White, *Am. J. Physiol. Cell. Physiol.*, 2008, **295**, C1037.
47 M. J. Berridge, *Cell Signalling Biology*, 2012, doi:10.1042/csb0001008

